Urinary ketone body loss leads to degeneration of brain white matter in elderly SLC5A8-deficient mice.

Laurent Suissa[1,2,3,4], Virginie Flachon[1,2,3,$], Jean-Marie Guigonis[1,2,3], Charles-Vivien Olivieri[1,2,3,£], Fanny Burel-Vandenbos[6], Julien Guglielmi[1,2,3], Damien Ambrosetti[6], Matthieu Gérard[7], Philippe Franken[1,2,3,5], Jacques Darcourt[1,2,3,5], Luc Pellerin[8,9], Thierry Pourcher[1,2,3,*] and Sabine Lindenthal[1,2,3,*]

[1]Laboratory Transporter in Imaging and Radiotherapy in Oncology (TIRO), University Nice Sophia Antipolis, 06107, Nice, France

[2]Laboratory Transporter in Imaging and Radiotherapy in Oncology (TIRO), Institut de biosciences et biotechnologies d'Aix-Marseille (BIAM), Commissariat a l'Energie Atomique, 06107, Nice, France

[3]Laboratory Transporter in Imaging and Radiotherapy in Oncology (TIRO), University Côte d'Azur, 06107, Nice, France

[4]Intensive care stroke unit, University Hospital, 06000, Nice, France

[5]Nuclear medicine department, Center Antoine Lacassagne, 06186, Nice, France

[6]Department of Pathology, University Hospital, 06000, Nice, France

[7]Institute for Integrative Biology of the Cell (I2BC), CEA, CNRS, Univ. Paris-Sud, Université Paris-Saclay, 91198, Gif-sur-Yvette, France

[8]Département de Physiologie, Université de Lausanne, Lausanne, Switzerland

[9]Centre de Résonance Magnétique des Systèmes Biologiques, UMR5536 CNRS, Université de Bordeaux, Bordeaux, France

*These authors contributed equally to this study

[$]Present address, Pulsalys SATT Lyon Saint-Etienne, 69625, Villeurbanne, France

[£]Present address, Laboratory MICORALIS EA7354, Faculté de chirurgie dentaire, Université Nice-Sophia-Antipolis, Nice, France ; Laboratory Unité de Thérapie Cellulaire et Génique (UTCG), Centre Hospitalier Universitaire de Nice, Hôpital Pasteur, 0600, Nice, France

Running title: Ketone body loss leads to brain degeneration

Keywords: SLC5A8, brain, white matter, kidney, ketone body

Corresponding author: Thierry Pourcher, TIRO, Faculté de Médecine, 28 Avenue de Valombrose, 06107 Nice Cedex 2, France. Phone: +33 493377712. Email: pourcher@unice.fr

Disclosure statement: The authors declare no potential conflict of interest.

Abstract:

SLC5A8 is sodium-coupled monocarboxylate and ketone transporter expressed in various epithelial cells. A putative role of SLC5A8 in neuroenergetics has been also hypothesized although its neuronal expression is controversial. To clarify this issue, we studied the cerebral phenotype of SLC5A8-deficient mice during aging. Elderly SLC5A8-deficient mice presented diffuse leukoencephalopathy characterized by intramyelinic oedema without demyelination suggesting chronic energetic crisis. Hypo-metabolism in the white matter of elderly SLC5A8-deficient mice have been found using 99mTc-hexamethylpropyleneamine oxime (HMPAO) single-photon emission CT (SPECT). Since the SLC5A8 protein could not be detected in the mouse brain, it was hypothesized that the leukoencephalopathy of aging SLC5A8-deficient mice is caused by the absence of slc5a8 expression in a peripheral organ, i.e., the kidney, where SLC5A8 is strongly expressed in proximal tubules. An hyper-excretion of the ketone β-hydroxybutyrate (BHB) in the urine of SLC5A8-deficient mice was observed by LC-MS and showed that SLC5A8-deficient mice suffer a cerebral BHB insufficiency. Elderly SLC5A8-deficient mice also present altered glucose metabolism. We propose that the renal loss of BHB leads to a chronic energetic deficiency in the brain of elderly SLC5A8-deficient mice who cannot counterbalance their glucose deficit by increasing the use of an alternative fuel (BHB). This study highlights the importance of alternative energetic substrates in neuroenergetics especially under condition of restricted glucose availability.

Introduction:

SLC5A8 was first identified by our group as a protein that was putatively involved in iodide metabolism [1]. In parallel, the human *Slc5a8* gene was associated, by Li and collaborators, with tumor suppressor function in colon cancer [2]. In 2004, two groups reported sodium-dependent inward currents induced by various monocarboxylates under voltage-clamp conditions with SLC5A8-expressing *Xenopus laevis* oocytes [3-5]. Based on this property, it was proposed that the main physiological roles of SLC5A8 are sodium-coupled lactate absorption in the kidney and butyrate absorption in the colon [4,6,7]. SLC5A8 expression was found in the apical membranes of various epithelial cell types (kidney, colon, thyroid and salivary glands). Frank and collaborators showed that SLC5A8-deficient mice are viable, fertile and they lack a morphological phenotype [7]. The same group demonstrated the role of SLC5A8 in lactate reabsorption in the kidney, salivary glands and colon. Despite its observed tumor suppressor function, SLC5A8-deficient mice did not show a higher incidence of colon tumor formation than control animals [7].

In the literature, evidence for the expression of SLC5A8 in brain remains unclear. Frank and collaborators did not detect SLC5A8 in mouse brain tissue [7], whereas Martin and collaborators reported neuron-specific expression and thus proposed that SLC5A8 functions as a Na^+-coupled transporter responsible for the active uptake of L-lactate and ketone bodies in neurons [8]. Recent advances in neuroenergetics demonstrated metabolic compartmentalization where astrocytes display more glycolytic activity, while neurons mostly rely on oxidative pathways. Consequently, the utilization of glucose, the major energy source of the brain [9], differs between the two cell types. According to the astrocyte neuron lactate shuttle hypothesis (ANLS), glucose is prominently utilized by astrocytes that feed neurons through the release of L-lactate, which is formed from pyruvate, the end product of glycolysis. Under normal physiological conditions, lactate is thought to be the preferred energy substrate of neurons [10]. Ketones are also capable of

fulfilling the energy requirements of the brain and can become the primary energetic fuel when the entry of glucose is impaired [11-16] as is the case in diabetes, during starvation and aging. Similar to the interaction between the astrocytes and neurons in L-lactate production and utilization, ketone bodies are also shuttled between astrocytes and neurons [17]. In the neurovascular unit, which is mainly composed of neurons, astrocytes and endothelial cells of the blood-brain barrier, the transport of monocarboxylates and ketone bodies is mediated by monocarboxylate transporters (MCTs). The expression of different members of the MCT family in each cell type of the neurovascular unit allows the flux of energetic substrates, not only through the blood-brain barrier, but also among brain parenchymal cells [18,19]. Since previous reports demonstrated that SLC5A8 is a Na^+-dependent transporter of monocarboxylates and ketone bodies [3-5,8] and given that neuronal expression of the protein has been observed, Martin and collaborators proposed a putative neuroenergetic role for SLC5A8 in the maintenance of energy status and neuron function [8].

Here, we used SLC5A8-deficient mice to understand the physiological role of the protein in the brain, particularly during aging.

Materials and Methods

Generation of SLC5A8-deficient mice

A neomycin-resistance cassette flanked by *loxP* sites and a *loxP* site were inserted upstream of the sixth exon and downstream of the seventh exon, respectively, at the *Slc5a8* locus. Embryonic stem (ES) cells (129Sv) were electroporated under standard conditions. Clones were selected for G418 resistance. We identified homologously-recombined clones and mutant mice by PCR and confirmed by Southern blot (using 3´ and 5´ probes). Four independent ES clones harboring the recombined allele were injected into C57BL/6 blastocysts. Chimeric males derived from two independent ES clones were bred with C57BL/6 females, and their progeny were analyzed by Southern blot. Mice homozygous for the modified *Slc5a8* locus were obtained. No obvious difference was detected, when compared to the parental mice. Females carrying the floxed-SLC5A8 allele in a mixed C57BL6/129Sv background were subsequently bred with a heterozygous Cre-transgenic male (mixed 129Sv/FVB), leading to the deletion of the sixth and seventh exons. The progeny were genotyped and mice carrying both the Cre transgene and the slc5a8 mutant allele were selected. First, males and females were mated to obtain mice carrying the slc5a8 allele but lacking the Cre transgene. These males and females were then mated to obtain homozygous SLC5A8-deficient mice. All study protocols were approved by our local Committee for Animal Studies and were consistent with the National Institute of Health principles of animal laboratory care (NIH publication 86-23, revised 1995). Animals were fed a standard diet. Mice with the same mixed background were used as controls and referred to as wild-type (WT). The animals were treated in accordance with the French Agriculture Ministry guidelines, and the experiments were approved by the University of Nice Sophia Antipolis Animal Care User and Ethics Committee (Ciepal NCE/2016–211 and APAFIS#4205-2016012714424849).

Histology

Mice were sacrificed by cervical dislocation. Brain and kidneys were rapidly removed and fixed in 3.7% (v/v) paraformaldehyde for 24 hours prior to paraffin embedding. Four μm slices were deparaffinized, rehydrated and pre-treated using automated PT link (Dako SA, Trappes, France). The slices were stained with HES (Hematoxylin 3 min, Eosin 30 s and Safran 15 min). Luxol fast blue coloration (for 12h at 56°C) was used to visualize myelin distribution. Image acquisitions were performed by light microscopy as described for the immunohistological experiments below.

Whole brains were rapidly removed from sacrificed animals and frozen in liquid nitrogen. Ten μm sections were prepared from frozen brains with a cryostat. Slices were placed on glass slides and stored at -20°C until required for LC-MS sample preparation. Specific parts of the slices (for example, the cortex) were carefully removed from the slide by scraping. The remaining tissue was then detached from the slides with 70% methanol and collected in 1.5 mL centrifuge tubes and incubated overnight at -20°C. Samples were then centrifuged at 13 000 g for 15 min at 4°C. Supernatants were removed and dried using a SpeedVac concentrator (SVC100H, SAVANT, Thermo Fisher Scientific, Waltham, MA, USA). Lyophilized samples were resuspended in 80 μL of a 20:80 acetonitrile-H_2O mixture (HPLC grade, Merck Millipore) and stored at -20°C until use for LC-MS analysis.

Immunohistochemistry

Mouse brain sections and kidneys were fixed in 3.7% formalin (in PBS for 24 hours), embedded in paraffin, and sectioned at 4 μm. Sections were deparaffinized, rehydrated and antigens retrieved (pH 6.0, 10 mM Na-citrate buffer) using a PT link (Dako SA, Trappes, France). Immunostaining was performed with the Dako Autostainer (Dako SA) following the manufacturer's standardized protocol for all steps.

Antibodies: the monoclonal anti-SLC5A8 antibody (see supplementary figure 1) was obtained by immunizing mice with purified peptides corresponding to the C-terminus domain of the mouse SLC5A8 and fusion of their splenocytes with a mouse myeloma cell line (ATCC®CRL-1580) according to standard protocols [20]. Anti-SLC5A8 antibody was used at 23.2 mg/L. Brain cell-specific antibodies included NeuN (1:50; Abcam), Olig2 (1:100; Abcam), GFAP (1:4000; Abcam) and Iba1 (1:500; RayBioteck). The secondary antibodies were EnViosion reagents (Dako SA), and were used following the manufacturer's instructions. All sections were counterstained with hematoxyline, rinsed in water, dehydrated and mounted with cover slips. Image acquisition was performed using ICS Framework software (TRIBVN, Chatillon, France) and a Nikon microscope (Nikon France Instruments, Champigny sur Marne, France) equipped with a Nikon Camera and motorized stage.

In vivo SPECT ^{99m}Tc-dl-HMPAO (hexamethylpropyleneamine oxime) imaging

SPECT (Single photon emission computed tomography) was used for *in vivo* imaging of mouse brains with the ^{99m}Tc-*dl*-HMPAO (hexamethylpropyleneamine oxime) perfusion tracer (CERESTAB™, GE Healthcare SAS, France). The ^{99m}Tc-HMPAO injection solutions were prepared for clinical use by the radio-pharmacy of the medical center for oncology Antoine Lacassagne (Nice) using a commercially available kit and following the manufacturers guidelines. Technetium pertechnetate eluate ($^{99m}TcO_4^-$) was produced by a ^{99m}Tc-generator at the radio-pharmacy. HMPAO is a lipophilic compound, and intravenous administration was required to obtain optimal cerebral capture of the tracer. For stability reasons, the HMPAO solution was prepared within two hours prior to injection. 100 to 150 MBq in 0.25 mL 0.9% NaCl was injected in the animal's caudal vein using a 29-gauge (13 × 0.33 mm) needle. The true activity of the injected dose was calculated by measuring the activity in the syringe before and after injection using a dosimeter calibrated for ^{99m}Tc. Thirty minutes after injection, mice were anesthetized with 1.5% Isoflurane* under respiratory monitoring before starting the

imaging procedure. Imaging was performed with a semiconductor gamma camera and multi-pinholes coupled to a General Electric CT Scanner (eXplore speCZT CT120). The imaging procedure started with the tracking sequence (SCOUT) followed by the SPECT acquisition, coupled to the CT scanner (X-ray tube parameters: 100 kV voltage, 50 mA current) for 30 minutes. Image analysis was performed using the Amide software (A Medical Image Data Examiner version 1.0.4) [21]. Native values of SPECT imaging were expressed as a percentage of injected activity per volume of tissue. For this, the activity present in the animal at the time of imaging was calculated from the injected activity corrected for the period of imaging. This value was calculated as follows: activity injected, the imaging timeframe, the decay formula radioactivity and the half-life of ^{99m}Tc (6.005 hours). CT scanner imaging provides only bone information for the mouse cranial box, acquired images have been fused with the anatomical atlas digital brain of the adult mouse C56Bl/6 to perform measurement of radioactivity in different brain anatomical regions [22]. All values obtained have been normalized and are given as a percentage of the average cerebral HMPAO uptake.

Because blood flow in the brain is tightly coupled to local brain metabolism and energy use, ^{99m}Tc-*dl*-HMPAO uptake was used to assess regional brain metabolism.

Urine collection

Male mouse littermates (three per cage) were housed collectively in a mouse metabolic cage (Techniplast, Germany) with free access to water and standard mouse chow. After adaptation to the cage for a maximum of 48 hours or until no weight loss was detected, urine was collected over a period of 24 hours and stored at -20°C until use.

LC-MS analysis

24-hour urine samples were mixed with 3 volumes of methanol and incubated overnight at -20°C for protein precipitation. Samples were then centrifuged at 13 000 g for 15 min at 4°C. Supernatants were removed and dried using a SpeedVac concentrator (SVC100H, SAVANT, Thermo Fisher Scientific, Waltham, MA, USA). Lyophilized samples were resuspended in 80 μL of a 20:80 acetonitrile-H_2O mixture (HPLC grade, Merck Millipore) and stored at -20°C until use for LC-MS analysis.

- ***HPLC (High Pressure Liquid Chromatography)***

Chromatographic analysis was performed with the DIONEX Ultimate 3000 HPLC system coupled to a chromatographic column (Phenomenex Synergi 4 u Hydro-RP 80A 250x3.0 mm) set at 40°C and a flow rate of 0.9 mL/min. Gradients of mobile phases (mobile phase A: 0.1% formic acid in water and mobile phase B: 0.1% formic acid in acetonitrile) over a total of 25 minutes were as follow: 0 min (100% A; 0% B), 5 min (100% A; 0% B), 21 min (5% A; 95% B), 21.5 min (5% A; 95% B), 22 min (0% A; 100% B) and 25 min (0% A; 100% B).

- ***Mass Spectrometry***

MS analysis was carried out on a Thermo Scientific Exactive Plus Benchtop Orbitrap mass spectrometer. The Heated Electrospray Ionization source (HESI II) was used in positive (spray voltage at 3800 V) and negative ion modes (spray voltage at 2500 V). The vaporizer temperature was 350 °C and the ion sweep gas was 1.0 units. The temperature of the ion transfer tube temperature was 300 °C. Sheath gas pressure (N2) was 60 units and the auxiliary gas pressure (N2) was 15 units. With the Exactive Plus Benchtop Orbitrap mass spectrometer, generic conditions and an external mass calibration were applied. The instrument was operated in full scan mode from *m/z* 67 to *m/z* 1000. High-resolution accurate mass (HRAM) full-scan MS and top 5 MS/MS spectra were collected in a data-dependent fashion at a resolving power of 70,000 and 35,000 at FWHM *m/z* 200, respectively. The Stepped NCE (Normalized Collision Energy) setting was 40. Raw data files were converted to mzXML files using MSconvert

(version 2.1, ProteoWizard) [23]. The post-treatment of data was performed using the MZmine 2 version 2.31 (Boston, United States). Metabolites were identified using the Human Metabolome Database version 4.0 (HMDB).

Microarray experiments and statistical analysis

RNA was isolated with a RNeasy kit (Qiagen, Courtaboeuf, France) from freshly removed mouse brain tissue according to the manufacturer's protocol. RNA samples were labeled with Cy3 dye using the Low RNA Input QuickAmp Kit (Agilent), as recommended by the supplier. Labelled cRNA probes (400 ng) were hybridized on 8x60K high-density SurePrint G3 gene mouse GE 8x60K Agilent microarrays. Four biological replicates were performed for each experimental condition. The experimental data are deposited in the NCBI Gene Expression Omnibus (GEO) (http://www.ncbi.nlm.nih.gov/geo/) under the record number, GSE117705. Normalization of microarray data was performed using the Limma package (http://www.bioconductor.org). Interslide normalization was performed using the quantile methods. Means of ratios from SLC5A8-deficient versus control tissues were calculated and B-test analysis was performed. Differentially expressed genes were selected based on an adjusted p value of 0.05. Data from expression microarrays were analyzed for enrichment in biological themes (Gene Ontology molecular function and canonical pathways) and biological networks were built using Ingenuity Pathway Analysis software (http://www. ingenuity.com/).

Intra-peritoneal glucose and insulin tolerance tests

For glucose tolerance tests (GTT), mice were injected intraperitoneally with 2 g glucose (Sigma) per kg of body weight in 0.9% NaCl after an overnight fast (16h). For insulin tolerance tests (ITT), mice were starved for 6h and injected with 0.75 IU/kg body weight of soluble insulin (Humulin Regular; Eli Lilly & Co., Indianapolis, Indiana, USA). Blood glucose levels

were measured before (t=0) and after glucose/insulin injection at 15, 30, 60 and 120 minutes. Glycemia was measured on venous blood samples from the tail vein using a Glucometer OneTouch Verio (LifeScan Inc., Canada).

Statistical analyses

Statistical analyses were performed using Microsoft Excel software for all experiments. Results were expressed as the means +/- of the standard errors. Student's *t*-tests were used to compare different conditions. A p value of < 0.05 was considered to be significant.

Results

Immunohistology of SLC5A8-deficient and wild-type mouse brains.

The histological phenotype of 4-, 12- and 20-month-old SLC5A8-deficient mice (KO) was examined and compared to wild-type mice (WT). Hematoxylin and eosin (H&E) staining of sagittal brain slices revealed large vacuoles with spongiotic appearance throughout the white matter of the cerebellar arbor vitae of 20-month-old SLC5A8-deficient mice. These vacuoles were not detected in the brains of 20-month-old wild-type mice. They were not observed either in brains of 12-month-old mice and 4-month-old mice, SLC5A8-deficient nor controls **(Figure 1A).** Using luxol fast blue staining (FBL), no myelin loss was found in the cerebellar arbor vitae of all SLC5A8-deficient mice compared to wild-type mice indicating normal myelination and myelin maintenance **(Figure 1A)**. Because empty vacuoles, at high magnification, were crossed by fine luxol-stained tissue strands, we concluded that these vacuoles may be located within myelinic regions. Furthermore, myelin bundles of large fiber tracts in the brainstems of SLC5A8-deficient mice were found to be distorted, suggesting myelin sheath swelling **(Figure 1B)**. Segmental intramyelinic oedema without myelin loss was detected in all other brain regions containing white matter (corpus callosum, internal capsule, pencils of Wilson, fiber bundles of caudoputamen and brainstem). According to the intramyelinic location of vacuoles, no vacuole was observed in the gray matter (cortical or cerebellar cortex) of these animals **(Figure 1C)**. In addition, no cytoplasmic vacuole was revealed in oligodendrocytes and neurons by immunostaining with anti-Olig2 antibodies and anti-NeuN antibodies, respectively **(Figure 1C)**. Microglia was studied by immunostaining using anti-Iba1 antibodies. In 20-month-old SLC5A8-deficient mice, iba1-positive staining revealed the activation of microglial cells characterized by amoeboid morphology and increased cell volume. In wild-type mice and in young null mice, iba1 staining revealed the "resting" phenotype of microglial cells with a relatively small cellular body and long branching extensions **(Figure 1D)**. Iba1 immunostaining

of coronal sections from caudal-diencephalon regions showed microglial activation of white matter areas only in 20-month-old SLC5A8-deficient mice. Therefore, we concluded that elderly SLC5A8-deficient mice present diffuse leucoencephalopathy characterized by segmental intramyelinic oedema without myelin loss and associated to microglial activation.

In vivo SPECT imaging with ^{99m}Tc-dl-HMPAO (hexamethylpropyleneamine oxime) of SLC5A8-deficient and wild-type mouse brains

Because blood flow in the brain is tightly coupled to local brain metabolism and energy consumption, ^{99m}Tc-*dl*-HMPAO (hexamethylpropyleneamine oxime) perfusion tracer was used to assess regional brain metabolism. It has to be noted that brain ^{18}F-FDG (fluorodeoxyglucose) PET imaging could have been a possible alternative approach but it was not used since it can only assessed cerebral glucose metabolism. Cerebral ^{99m}Tc-*dl*-HMPAO (CERESTAB*) uptake was measured by SPECT imaging in SLC5A8-deficient and wild-type mice aged 4 and 12 months, respectively. ^{99m}Tc-*dl*-HMPAO uptake was measured in the neocortex, caudo-putamen, thalamus as well as the cerebellum and normalized to the mean brain uptake **(Figure 2)**. No difference in gray matter HMPAO uptake, represented by the neocortex and thalamus regions, was detected between SLC5A8-deficient and wild-type mice at both ages. In contrast, mixed brain structures containing gray and white matter-like caudo-putamen and cerebellum, presented significant hypoperfusion in 12-month-old SLC5A8-deficient mice when compared to wild-type mice at the same age **(Figure 2)**. Since hypoperfusion was only found in mixed brain structures, we concluded that the alterations to cerebral energy metabolism in 12-month-old SLC5A8-deficient mice were limited to the brain white matter.

Expression of SLC5A8 in wild-type mice

To further analyze SLC5A8 expression in different brain regions of wild-type mice, immunohistochemistry was performed with a novel anti-SLC5A8 antibody that we generated and characterized (supplementary figure 1). No SLC5A8-specific staining was detected in the brains of 3-month and 20-month-old control mice nor in SLC5A8-deficient mouse brains at the same ages **(Figure 3A)**. In contrast, strong SLC5A8-specific staining was revealed with the same anti-SLC5A8 antibody in the kidney of 3-month-old wild-type mice while it was not detected in the kidney of 3-month-old SLC5A8-deficient mice, as expected **(Figure 3B)**. In accordance with the literature, expression of the SLC5A8 protein was typically localized in the brush border of proximal convoluted tubules in the kidney of wild-type mice.

LC-MS analyses of 24-hour urine from SLC5A8-deficient and wild-type mice.

Since the SLC5A8 protein was not detected in the brain of wild-type mice, it was hypothesized that the observed cerebral phenotype of SLC5A8-deficient mice could be associated with a systemic effect due to the loss of energetic substrates during renal filtration. Frank and collaborators reported lactaturia in SLC5A8-deficient mice but the authors found no alteration in plasma L-lactate levels in these mice compared to control animals [7]. Similar to L-lactate, ketones are considered to be the brain's main alternative energy source to glucose [13] but no information about their circulating and/or tissue levels as well as their excreted amounts have been reported in SLC5A8-deficient mice.

The physiological role of the SLC5A8 protein in renal reabsorption was studied through a comparison of the urinary metabolome of wild-type and SLC5A8-deficient mice. Twenty-four-hour urine collections from null mice and control animals were analyzed by LC-MS. β-hydroxybutyrate (see supplementary figure 2 for its mass spectrometry identification) was found to be significantly increased in the 24h urine of SLC5A8-deficient mice compared to wild-type mice. KO/WT ratios of this ketone body were higher for 18-month-old mice

(approximately 12-fold) than for 3-month-old mice (approximately 7-fold; **Figure 4A**). No difference was noted for the urinary creatinine levels between all animals (Supplementary figure 3A), which allowed us to make the above comparison without normalization. As described by Frank and collaborators [7], we found lactaturia in SLC5A8-deficient mice (3.5-fold; Supplementary figure 3B) and also an increased level of pyruvate in the urine of SLC5A8-deficient mice compared to control animals (5.7-fold; Supplementary figure 3B).

Hydroxybutyryl-carnitine, the ester of hydroxybutyryl and carnitine, is the activated form of β-hydroxybutyrate. Because the level of this acyl carnitine was known to be correlated with the systemic level of its derived short chain fatty acid, the systemic consequence of β-hydroxybutyrate loss in SLC5A8-deficient mouse urine was determined by analysis of β-hydroxybutyryl-carnitine [24]. The level of the acyl-carnitine form of β-hydroxybutyrate was found to be significantly decreased in SLC5A8-deficient mice versus control mice in 24-hour urine samples suggesting a systemic impact due to ketone body loss in the urine of SLC5A8-deficient mice. No significant difference was observed for the KO/WT ratio of hydroxybutyryl-carnitine (see supplementary figure 4 for its mass spectrometry identification) between 3-month-old mice (≈12-fold) and 18-month-old mice (≈8-fold; **Figure 4B**). The level of two additional ketones, acetoacetate and acetone, could not be detected by LC-MS. Acetoacetate was assessed by a semi-quantitative urinalysis reagent test (Legall method). This colorimetric test gave positive staining for high levels of acetoacetate in the urine of SLC5A8-deficient mice, while the test was negative (no staining) for the urine of wild-type mice. In conclusion, SLC5A8-deficient mice showed a defect in renal reabsorption of both major ketone bodies.

LC-MS analyses of SLC5A8-deficient and wild-type mouse brains.

Since SLC5A8-deficient mice presented strong ketonuria, cerebral β-hydroxybutyrate levels in SLC5A8-deficient mice were compared to those of wild-type mice using an LC-MS approach.

First, β-hydroxybutyrate levels were measured in homogenized whole brains of 24 month-old mice. SLC5A8-deficient mouse brains contained 28% less β-hydroxybutyrate than brains of control animals **(Figure 5A)**. Second, the levels of β-hydroxybutyrate were assessed in different cerebral areas. To exclude the possibility that the previously described results are due to aging, 6-month-old mice were used for these experiments. Rostral-mesencephalon brain sections were chosen including the occipital neo-cortex (grey matter) and the mesencephalon (white matter) **(Figure 5B)**. The level of β-hydroxybutyrate was 27% lower in coronal mesencephalon sections of SLC5A8-deficient mice than in the same brain sections of control animals. It can be concluded that SLC5A8-deficient mice suffer from low cerebral β-hydroxybutyrate levels, particularly in the white matter, most probably due to the loss of ketone bodies via the urine. This phenomenon was not a consequence or result of aging.

Transcriptomic analyses on SLC5A8-deficient and wild-type mouse brains.

In the brain, ketones are produced by ketogenic amino acid and fatty acid breakdown in astrocytes. Transcriptomic analyses (NCBI GEO platform Accession Number GSE117705) on whole brain homogenates were performed from SLC5A8-deficient and wild-type mice at ages of 4 and 18 months to study the expression of genes encoding proteins that are involved in ketogenic amino acid and lipid catabolism [25-28].

No significant up-regulation of *BCAT2, Aass and Tdo2* was found in slc5a8-null mice at 4 and 18 months of age. These genes encode proteins involved in the degradation of the ketogenic amino acids leucine, lysine and tryptophan. *BCAT2* encodes the mitochondrial enzyme "branched chain amino acid transaminase 2", which catalyzes the first step of the leucine degradation pathway leading to the production of acetyl-CoA, acetoacetate and β-hydroxybutyrate. *Aass* stands for aminoadipate-semialdehyde synthase, a bifunctional enzyme responsible for the first two steps of the lysine degradation pathway. *Tdo2*, or tryptophan 2,3-

dioxygenase, catalyzes the first and rate-limiting step of tryptophan catabolism. The *Pts* gene product, 6-pyruvoyltetrahydropterin synthase, is involved in the transformation of the ketogenic amino acids phenylalanine, tyrosine and tryptophan into non-energetic degradation products. *Pts* was found to be down-regulated in SLC5A8-deficient mice suggesting metabolic reorientation that may allow for the production of ketones from these amino acids instead of non-energetic molecules. In addition, an up-regulation of *LAT4 (SLC43A2)* expression was found in SLC5A8-deficient mice but this finding was limited to 18-month-old animals. Interestingly, the *LAT4* gene encodes a member of the amino acid transporter-3 family (SLC43), which mediates the transport of branched-chain amino-acids including leucine. Taken together, these results show enhanced transcription of genes encoding proteins that are involved in ketogenic amino-acid catabolism and transport in the brain of SLC5A8-deficient mice. This finding suggests that increased ketogenic amino acid catabolism and ketone production in the brain of these animals may serve to compensate for urinary ketone loss.

Phospholipase A_2 (*Pla2g4e*) gene transcripts were observed to be up-regulated in the brain of SLC5A8-deficient mice of both ages when compared to brains of corresponding control mice. Phospholipase A_2 found in brain tissue has been associated with the $cPLA_2$-sphingomyelinase pathway in which brain lipids are utilized to generate fatty acids. In astrocytes, fatty acids are converted into ketone bodies to fulfil the energy needs of neurons [28]. In 18-month-old SLC5A8-deficient mice, the level of transcripts from two additional genes encoding lipolytic enzymes, phospholipase C (*Plcd4*) and phospholipase D2 (*Pld2*) were also up-regulated when compared to control mice.

It is concluded that, in SLC5A8-deficient mice, the ketogenic amino-acid and lipid catabolism pathways are activated as an adaptive compensatory response to β-hydroxybutyrate deficiency in the brain. As would be expected, this compensatory mechanism intensified in the aging brain.

In addition, enhanced levels of *Fxyd2* gene transcripts coding for an auxiliary subunit of the Na^+-K^+-ATPase were detected in SLC5A8-deficient elderly mice. FXYD2 proteins regulate Na^+-K^+-ATPase activity by increasing the apparent affinity of the transporter for ATP, while decreasing its Na^+ affinity. Increased expression of the *Fxyd2* gene occurs in order to maintain the Na^+-K^+-gradient across the plasma membrane when ATP production is low [29]. This finding is in accordance with our hypothesis that SLC5A8-deficient mice struggle to meet the energy demands of the brain, particularly during aging.

Glucose and insulin tolerance tests (GTT/ITT) in young and elderly SLC5A8-deficient and wild-type mice.

We previously showed that SLC5A8-deficient mice exhibit white matter degeneration in the aging brain that is most probably linked to ketone body deficiency. The principal reason for ketone bodies to become the primary energy source in the brain is because of reduced availability of glucose for brain cells, as occurs during prolonged starvation or diabetes, for example. Our animals had free access to drinking water and food, and did not suffer starvation. Therefore, glucose metabolism was assessed by performing glucose tolerance tests (GTT) on 3-month and 18-month-old SLC5A8-deficient and control mice. These tests did not reveal any glucose metabolism disorder in young SLC5A8-deficient mice vs. control mice **(Figure 6A, 6B)**. In contrast, aged SLC5A8-deficient mice displayed significantly higher (170.3±11.1 mg/dL) overnight fasting capillary glycaemia compared to control mice (139.6±6.1 mg/dL). GTT in aged SLC5A8-deficient mice revealed that blood glucose levels following an intra-peritoneal glucose injection were significantly higher than in controls, suggesting glucose intolerance (**Figure 6A**). ITT was performed on the same SLC5A8-deficient mice that presented glucose intolerance. ITT is an established method for quantifying insulin resistance that may be at the origin of the observed glucose intolerance in SLC5A8-deficient mice. Our

results showed that the decay rate of capillary glycaemia was not significantly lower in elderly SLC5A8-deficient mice leading us to conclude that these mice presented glucose intolerance due to islet function but not insulin action **(Figure 6C)**. In accordance with this conclusion, elderly SLC5A8-deficient mice had a significantly smaller body weight than control mice **(Figure 6D)**.

Discussion:

Here we report, for the first time, that aged SLC5A8-deficient mice present a cerebral ketone body deficiency due to a defect in renal ketone reabsorption. Ketone bodies are an alternative energy source for the brain, particularly when the glucose supply is impaired. Our studies showed that aging SLC5A8-deficient mice exhibit brain white matter lesions. This cerebral phenotype is most probably due to a chronic energy deficit caused by ketone deficiency and glucose intolerance. This report highlights the major role of ketones in terms of neuroenergetics and neuroprotection for the elderly.

Aged SLC5A8-deficient mice show diffuse leucoencephalopathy characterized by intramyelinic oedema without myelin loss associated with microglial activation. According to Van Der Knaap's classification of myelin disorders, intramyelinic oedema without myelin loss is associated with metabolic disorders [30]. Intramyelinic oedema is commonly referred to as a water/ion homeostasis disorder in peri-axonal regions or between lamellae, the so-called "panglial syncytium". Strong evidence has suggested that alterations in the "panglial syncytium" could lead to myelin ultra-structural lesions with intramyelinic oedema [31]. Studies of transgenic knockout mouse models for connexins 43/30, Kir 4.1, ClC2 or GlialCAM (a ClC2 chaperone) have reported an intramyelinic oedema phenotype in the brain [32-36]. In humans, loss-of-function mutations in ClC2 lead to megalencephalic leukoencephalopathy with subcortical cysts, a disease characterized by chronic brain white matter vacuolar oedema [37,38]. Interestingly, chronic brain hypoperfusion models also lead to segmental intramyelinic oedema in the white matter [34]. In TgPAC-Notch3^{R169C} mice, a pre-clinical mouse model of small vessel disease named CADASIL (Cerebral Autosomal Dominant Arteriopathy with Subcortical Infarctus and Leukoencephalopathy), early changes in white matter are linked to intramyelinic oedema with microglial activation [39]. We observed similar changes in the white matter of our aging SLC5A8-deficient mice as those described by Wakita and collaborators with a chronic hypoperfusion

mouse model obtained by the permanent bilateral occlusion of common carotid arteries [40]. Since brain hypoperfusion is associated with energy deficit, this finding suggests that the intramyelinic oedema and glial activation are associated with chronic energy deficiency. In a mouse model for maple syrup urinary disease, an inherited disorder of branched-chain amino acid metabolism, vacuolization and disruption of white matter was reported and attributed by the authors, in part, to long-term cerebral energy deprivation [41]. For several groups, these histological lesions might be the consequences of a water/ion homeostasis defect in the "panglial syncytium" due to the failure of key ATP-dependent ion pumps [31, 39, 41]. Our SPECT HMPAO study of brain regional metabolism also supports the hypothesis that chronic energetic failure leads to intramyelinic oedema with glial activation.

Martin and collaborators [8] remains the only group that reported widespread expression of the SMCT1 mRNA in the mouse brain by *in situ* hybridization analysis. Specific expression was illustrated at higher magnification in the cortex and hippocampus. They also performed immunofluorescence analysis and proposed that the SMCT1 protein is expressed exclusively in neurons. Results shown in this publication are in contrast with our results presented here and all other analyses performed up to now on SLC5A8 expression in the mouse brain. First, Frank and collaborators [7] did not observe SLC5A8 expression in the mouse brain by *in situ* hybridization analysis and western blot. The same conclusion was supported by data from the Allen mouse brain atlas (http://mouse.brain-map.org) obtained by ISH in the mouse brain [42]. Furthermore, in a RNA-sequencing transcriptome database (http://www.brainrnaseq.org) of glia, neurons, and vascular cells of the mouse or human brain, transcripts of slc5a8 were not found [43,44]. Other RNA-sequencing databases like the expression atlas (http://www.ebi.ac.uk/gxa) gave the same result [45]. In a proteomic study of membrane proteins in different areas of the rat brain, no peptide corresponding to the SLC5A8 protein was found despite the identification of a large number of membrane proteins [46]. At last, the absence of a brain phenotype during the

entire developmental and adult period of the KO mouse do not support the presence of SLC5A8 expression in brain. Therefore, we hypothesize that the white matter phenotype of aging SLC5A8-deficient mice underlies a metabolic disorder which is caused by the lack of SLC5A8 expression in a peripheral organ (and not by a lack of cerebral expression). We assume that chronic brain energetic failure, demonstrated by prototypic histological lesions and energetic metabolism disturbances using SPECT HMPAO in the white matter of elderly SLC5A8-deficient mice, was in fact the result of the loss of energetic substrates in urine. In accordance with the literature, we showed that SLC5A8 is strongly expressed in the kidney proximal tubule, which is the major resorptive segment of the nephron [4-7]. In addition, SLC5A8 is known to mediate sodium-dependent transport of monocarboxylates and ketone bodies leading us to assume that the renal reabsorption defect of these metabolites gives rise to an energy deficiency in the brain of aging SLC5A8-deficient mice [3-5,8,47]. *In vivo*, LC-MS analyses of 24-hour urine confirmed lactaturia in SLC5A8-deficient mice, as described by Frank and collaborators [7], and it was further supported by increased urinary levels of other monocarboxylates. But most interestingly, these studies showed strong hyper-excretion of the ketone body β-hydroxybutyrate in the urine of SLC5A8-deficient mice. We then turned to consider the systemic effects of this strong β-hydroxybutyrate loss, and the consequences for the brain. Interestingly, the serum levels of ketone bodies were not affected by the renal loss. However, the acyl-carnitine form of β-hydroxybutyrate (i.e., hydroxybutyryl-carnitine) was found to be significantly decreased in 24-hour urine of SLC5A8-deficient mice. Because the level of this acyl carnitine is known to be correlated with the systemic level of its derived short chain fatty acid [24], we therefore conclude that, despite the constant serum level, the loss of β-hydroxybutyrate through urine in SLC5A8-deficient mice has significant effects on its availability for the energy metabolism of these animals.

Our data clearly show that SLC5A8-deficient mice suffer β-hydroxybutyrate insufficiency in the white matter, while normal levels were obtained for the grey matter. This may be due to more efficient β-hydroxybutyrate uptake across the blood-brain barrier in cortical regions where monocarboxylate transporters are more abundant [27, 48, 49]. It has been shown in a human brain ischemic model that white matter is more vulnerable to energy crisis than grey matter [50]. Whole-brain transcriptomic data showed that SLC5A8-deficient mice activate degradation of ketogenic amino-acids, leucine in particular, and that lipids most probably compensate for the β-hydroxybutyrate deficiency caused by urinary ketone loss. In accordance with our results, Klosinski and collaborators recently proposed that lipolysis of myelin lipids in the brain is an adaptive response that generates ketone bodies to fulfil the energy needs of neurons [28]. The authors presented evidence that the loss of myelin sheath integrity, observed only by electronic microscopy, is induced by activation of the $cPLA_2$-sphingomyelinase pathway [28]. Consistently, our SLC5A8-deficient mice presented enhanced expression of phospholipase A_2 in the brain, which is most likely an indication of increased lipolysis.

Despite the permanent loss of ketone bodies, starting from an early age, only elderly SLC5A8-deficient mice showed cerebral metabolism disturbances and detectable histological lesions by light microscopy in the white matter. SLC5A8-deficient mice cannot rely on the neuroprotective function of ketone bodies in the brain. In younger animals, neuroprotection may be a minor physiological function of ketones and compensatory systems could account for the absence of metabolic disorders or histological alterations in the brain. During aging, the neuroprotective function of ketones may become more important because cells are exposed to impaired glucose entry, increased oxidative stress and a pro-inflammatory environment [27, 28, 51]. Notably, we found that glucose metabolism was altered in elderly SLC5A8-deficient mice when compared to control animals. We suggest that glucose intolerance in elderly SLC5A8-deficient mice, in addition to permanent ketone body insufficiency, leads to a chronic energy crisis in the

brain of aging SLC5A8-deficient mice. The elucidation of the molecular mechanisms underlying glucose intolerance in elderly SLC5A8-deficient mice needs further investigation. We propose that the glucose intolerance found in elderly SLC5A8-deficient mice was the consequence of chronic ketogenesis induced by ketone body urinary loss as previously suggested [52].

Conclusions

In summary, we describe, for the first time, a mouse model for ketone body insufficiency. The presented results, in particular the alterations to the brain white matter of these animals, highlight the major roles of ketones as alternative energy substrates and in neuroprotection when glucose metabolism is impaired due to insulin resistance and aging. At present, studies of the physiological roles of ketones are limited to animal injury models or to human cases of traumatic, ischemic or neurodegenerative diseases with the application of various ketone administration protocols or ketogenic diets [27]. We provide here a new mouse model with permanent ketone deficiency that should be very useful in the development of novel neuroprotective agents in the case of brain injury or aging.

Acknowledgements:

This work was funded by grants of the “Commissariat à l’Energie Atomique" (“Programme de Toxicologie nucléaire”), the “Département des Alpes-Maritimes” (“Appel d’offre Santé”) and the “Commissariat Général à l’Investissement” (“Recherche en matière de Sûreté Nucléaire et Radioprotection” program operated by the ‘‘Agence Nationale de la Recherche’’ (ANR), France) and. LP received financial support from the program IdEx Bordeaux ANR-10-IDEX-03-02. We thank the IRCAN Animal Core Facility and the CHU Histology core facility for providing access to their equipment. The IRCAN Animal core facility is supported by the

University Nice Sophia Antipolis. Metabolomics analyses has been funded in by Cancéropole PACA and the Département des Alpes-Maritimes. We also thank Lyse Domenech, Marianne Goracci, Sandrine Destrée and Arnaud Borderie for excellent technical assistance. The authors acknowledge the excellent support of the Nice-Sophia Antipolis Functional Genomics Platform in which the microarray experiments were carried out. The authors wish to thank Abby Cuttris for critical reading of the manuscript.

References:

1. Rodriguez AM, Perron B, Lacroix L, et al. Identification and characterization of a putative human iodide transporter located at the apical membrane of thyrocytes. *J Clin Endocrinol Metab* 2002; 87: 3500-3503. DOI: 10.1210/jcem.87.7.8797.
2. Li H, Myeroff L, Smiraglia D, et al. SLC5A8, a sodium transporter, is a tumor suppressor gene silenced by methylation in human colon aberrant crypt foci and cancers. *Proc Natl Acad Sci U S A* 2003; 100: 8412-8417. DOI: 10.1073/pnas.1430846100.
3. Coady MJ, Chang MH, Charron FM, et al. The human tumour suppressor gene SLC5A8 expresses a Na+-monocarboxylate cotransporter. *J Physiol* 2004; 557: 719-731.
4. Gopal E, Fei YJ, Sugawara M, et al. Expression of slc5a8 in kidney and its role in Na(+)-coupled transport of lactate. *J Biol Chem* 2004; 279: 44522-44532. DOI: 10.1074/jbc.M405365200.
5. Miyauchi S, Gopal E, Fei YJ, et al. Functional identification of SLC5A8, a tumor suppressor down-regulated in colon cancer, as a Na(+)-coupled transporter for short-chain fatty acids. *J Biol Chem* 2004; 279: 13293-13296. DOI: 10.1074/jbc.C400059200.
6. Gupta N, Martin PM, Prasad PD, et al. SLC5A8 (SMCT1)-mediated transport of butyrate forms the basis for the tumor suppressive function of the transporter. *Life Sci* 2006; 78: 2419-2425. DOI: 10.1016/j.lfs.2005.10.028.
7. Frank H, Groger N, Diener M, et al. Lactaturia and loss of sodium-dependent lactate uptake in the colon of SLC5A8-deficient mice. *J Biol Chem* 2008; 283: 24729-24737. DOI: 10.1074/jbc.M802681200.
8. Martin PM, Gopal E, Ananth S, et al. Identity of SMCT1 (SLC5A8) as a neuron-specific Na+-coupled transporter for active uptake of L-lactate and ketone bodies in the brain. *J Neurochem* 2006; 98: 279-288. DOI: 10.1111/j.1471-4159.2006.03878.x.
9. Pellerin L and Magistretti PJ. Neuroenergetics: calling upon astrocytes to satisfy hungry neurons. *The Neuroscientist : a review journal bringing neurobiology, neurology and psychiatry* 2004; 10: 53-62. 2004/02/28. DOI: 10.1177/1073858403260159.
10. Pellerin L and Magistretti PJ. Sweet sixteen for ANLS. *J Cereb Blood Flow Metab* 2011.
11. Courchesne-Loyer A, Croteau E, Castellano CA, et al. Inverse relationship between brain glucose and ketone metabolism in adults during short-term moderate dietary ketosis: A dual tracer quantitative positron emission tomography study. *J Cereb Blood Flow Metab* 2017; 37: 2485-2493. 2016/09/16. DOI: 10.1177/0271678X16669366.
12. Cunnane S, Nugent S, Roy M, et al. Brain fuel metabolism, aging, and Alzheimer's disease. *Nutrition* 2011; 27: 3-20. 2010/11/03. DOI: 10.1016/j.nut.2010.07.021.
13. Cunnane SC, Courchesne-Loyer A, Vandenberghe C, et al. Can Ketones Help Rescue Brain Fuel Supply in Later Life? Implications for Cognitive Health during Aging and the Treatment of Alzheimer's Disease. *Frontiers in molecular neuroscience* 2016; 9: 53. 2016/07/28. DOI: 10.3389/fnmol.2016.00053.
14. Gjedde A and Crone C. Induction processes in blood-brain transfer of ketone bodies during starvation. *Am J Physiol* 1975; 229: 1165-1169. 1975/11/01. DOI: 10.1152/ajplegacy.1975.229.5.1165.
15. Hawkins RA, Mans AM and Davis DW. Regional ketone body utilization by rat brain in starvation and diabetes. *Am J Physiol* 1986; 250: E169-178. 1986/02/01. DOI: 10.1152/ajpendo.1986.250.2.E169.
16. Hawkins RA, Williamson DH and Krebs HA. Ketone-body utilization by adult and suckling rat brain in vivo. *Biochem J* 1971; 122: 13-18. 1971/03/01.
17. Guzman M and Blazquez C. Ketone body synthesis in the brain: possible neuroprotective effects. *Prostaglandins Leukot Essent Fatty Acids* 2004; 70: 287-292. 2004/02/11. DOI: 10.1016/j.plefa.2003.05.001.
18. Pellerin L, Halestrap AP and Pierre K. Cellular and subcellular distribution of monocarboxylate transporters in cultured brain cells and in the adult brain. *Journal of Neuroscience Research* 2005; 79: 55-64.

19. Pierre K and Pellerin L. Monocarboxylate transporters in the central nervous system: distribution, regulation and function. *J Neurochem* 2005; 94: 1-14. 2005/06/15. DOI: 10.1111/j.1471-4159.2005.03168.x.
20. de StGroth SF and Scheidegger D. Production of monoclonal antibodies: strategy and tactics. *J Immunol Methods* 1980; 35: 1-21.
21. Loening AM and Gambhir SS. AMIDE: a free software tool for multimodality medical image analysis. *Mol Imaging* 2003; 2: 131-137.
22. Li X, Aggarwal M, Hsu J, et al. AtlasGuide: software for stereotaxic guidance using 3D CT/MRI hybrid atlases of developing mouse brains. *J Neurosci Methods* 2013; 220: 75-84. 2013/09/03. DOI: 10.1016/j.jneumeth.2013.08.017.
23. Holman JD, Tabb DL and Mallick P. Employing ProteoWizard to Convert Raw Mass Spectrometry Data. *Current protocols in bioinformatics* 2014; 46: 13 24 11-19. 2014/06/19. DOI: 10.1002/0471250953.bi1324s46.
24. Soeters MR, Serlie MJ, Sauerwein HP, et al. Characterization of D-3-hydroxybutyrylcarnitine (ketocarnitine): an identified ketosis-induced metabolite. *Metabolism* 2012; 61: 966-973. 2012/01/03. DOI: 10.1016/j.metabol.2011.11.009.
25. Auestad N, Korsak RA, Morrow JW, et al. Fatty acid oxidation and ketogenesis by astrocytes in primary culture. *J Neurochem* 1991; 56: 1376-1386. 1991/04/01.
26. Bixel MG and Hamprecht B. Generation of ketone bodies from leucine by cultured astroglial cells. *J Neurochem* 1995; 65: 2450-2461. 1995/12/01.
27. White H and Venkatesh B. Clinical review: ketones and brain injury. *Critical care (London, England)* 2011; 15: 219. 2011/04/15. DOI: 10.1186/cc10020.
28. Klosinski LP, Yao J, Yin F, et al. White Matter Lipids as a Ketogenic Fuel Supply in Aging Female Brain: Implications for Alzheimer's Disease. *EBioMedicine* 2015; 2: 1888-1904. 2016/02/05. DOI: 10.1016/j.ebiom.2015.11.002.
29. Arystarkhova E, Wetzel RK and Sweadner KJ. Distribution and oligomeric association of splice forms of Na(+)-K(+)-ATPase regulatory gamma-subunit in rat kidney. *Am J Physiol Renal Physiol* 2002; 282: F393-407. 2002/02/08. DOI: 10.1152/ajprenal.00146.2001.
30. van der Knaap MS. Magnetic resonance in childhood white-matter disorders. *Developmental medicine and child neurology* 2001; 43: 705-712. 2001/10/23.
31. Rash JE. Molecular disruptions of the panglial syncytium block potassium siphoning and axonal saltatory conduction: pertinence to neuromyelitis optica and other demyelinating diseases of the central nervous system. *Neuroscience* 2010; 168: 982-1008. 2009/10/24. DOI: 10.1016/j.neuroscience.2009.10.028.
32. Neusch C, Rozengurt N, Jacobs RE, et al. Kir4.1 potassium channel subunit is crucial for oligodendrocyte development and in vivo myelination. *J Neurosci* 2001; 21: 5429-5438. 2001/07/24.
33. Lutz SE, Zhao Y, Gulinello M, et al. Deletion of astrocyte connexins 43 and 30 leads to a dysmyelinating phenotype and hippocampal CA1 vacuolation. *J Neurosci* 2009; 29: 7743-7752. 2009/06/19. DOI: 10.1523/JNEUROSCI.0341-09.2009.
34. Blanz J, Schweizer M, Auberson M, et al. Leukoencephalopathy upon disruption of the chloride channel ClC-2. *J Neurosci* 2007; 27: 6581-6589. 2007/06/15. DOI: 10.1523/JNEUROSCI.0338-07.2007.
35. Bugiani M, Dubey M, Breur M, et al. Megalencephalic leukoencephalopathy with cysts: the Glialcam-null mouse model. *Annals of clinical and translational neurology* 2017; 4: 450-465. 2017/07/12. DOI: 10.1002/acn3.405.
36. Hoegg-Beiler MB, Sirisi S, Orozco IJ, et al. Disrupting MLC1 and GlialCAM and ClC-2 interactions in leukodystrophy entails glial chloride channel dysfunction. *Nat Commun* 2014; 5: 3475. 2014/03/22. DOI: 10.1038/ncomms4475.
37. van der Knaap MS, Boor I and Estevez R. Megalencephalic leukoencephalopathy with subcortical cysts: chronic white matter oedema due to a defect in brain ion and water homoeostasis. *Lancet Neurol* 2012; 11: 973-985. 2012/10/20. DOI: 10.1016/S1474-4422(12)70192-8.

38. Depienne C, Bugiani M, Dupuits C, et al. Brain white matter oedema due to ClC-2 chloride channel deficiency: an observational analytical study. *Lancet Neurol* 2013; 12: 659-668. 2013/05/28. DOI: 10.1016/S1474-4422(13)70053-X.
39. Cognat E, Cleophax S, Domenga-Denier V, et al. Early white matter changes in CADASIL: evidence of segmental intramyelinic oedema in a pre-clinical mouse model. *Acta Neuropathol Commun* 2014; 2: 49. 2014/06/03. DOI: 10.1186/2051-5960-2-49.
40. Wakita H, Tomimoto H, Akiguchi I, et al. Glial activation and white matter changes in the rat brain induced by chronic cerebral hypoperfusion: an immunohistochemical study. *Acta Neuropathol* 1994; 87: 484-492. 1994/01/01.
41. Zinnanti WJ, Lazovic J, Griffin K, et al. Dual mechanism of brain injury and novel treatment strategy in maple syrup urine disease. *Brain* 2009; 132: 903-918. 2009/03/19. DOI: 10.1093/brain/awp024.
42. Lein ES, Hawrylycz MJ, Ao N, et al. Genome-wide atlas of gene expression in the adult mouse brain. *Nature* 2007; 445: 168-176. 2006/12/08. DOI: 10.1038/nature05453.
43. Zhang Y, Chen K, Sloan SA, et al. An RNA-sequencing transcriptome and splicing database of glia, neurons, and vascular cells of the cerebral cortex. *J Neurosci* 2014; 34: 11929-11947. 2014/09/05. DOI: 10.1523/JNEUROSCI.1860-14.2014.
44. Zhang Y, Sloan SA, Clarke LE, et al. Purification and Characterization of Progenitor and Mature Human Astrocytes Reveals Transcriptional and Functional Differences with Mouse. *Neuron* 2016; 89: 37-53. 2015/12/22. DOI: 10.1016/j.neuron.2015.11.013.
45. Petryszak R, Keays M, Tang YA, et al. Expression Atlas update--an integrated database of gene and protein expression in humans, animals and plants. *Nucleic Acids Res* 2016; 44: D746-752. 2015/10/21. DOI: 10.1093/nar/gkv1045.
46. Lu A, Wisniewski JR and Mann M. Comparative proteomic profiling of membrane proteins in rat cerebellum, spinal cord, and sciatic nerve. *J Proteome Res* 2009; 8: 2418-2425. 2009/03/18. DOI: 10.1021/pr8010364.
47. Ganapathy V, Thangaraju M, Gopal E, et al. Sodium-coupled monocarboxylate transporters in normal tissues and in cancer. *AAPS J* 2008; 10: 193-199. DOI: 10.1208/s12248-008-9022-y.
48. Pierre K, Magistretti PJ and Pellerin L. MCT2 is a major neuronal monocarboxylate transporter in the adult mouse brain. *J Cereb Blood Flow Metab* 2002; 22: 586-595. 2002/04/26. DOI: 10.1097/00004647-200205000-00010.
49. Halestrap AP and Wilson MC. The monocarboxylate transporter family--role and regulation. *IUBMB Life* 2012; 64: 109-119. DOI: 10.1002/iub.572.
50. Pantoni L, Garcia JH and Gutierrez JA. Cerebral white matter is highly vulnerable to ischemia. *Stroke* 1996; 27: 1641-1646; discussion 1647. 1996/09/01.
51. Gasior M, Rogawski MA and Hartman AL. Neuroprotective and disease-modifying effects of the ketogenic diet. *Behavioural pharmacology* 2006; 17: 431-439. 2006/08/31.
52. Ellenbroek JH, van Dijck L, Tons HA, et al. Long-term ketogenic diet causes glucose intolerance and reduced beta- and alpha-cell mass but no weight loss in mice. *Am J Physiol Endocrinol Metab* 2014; 306: E552-558. 2014/01/09. DOI: 10.1152/ajpendo.00453.2013.

Figure legends:

Figure 1: Elderly SLC5A8-deficient mice presenting regional metabolism disturbances in the cerebellum and caudoputamen. ^{99m}Tc-HMPAO regional distribution according to phenotype (slc5a8-deficient mice (KO) and control (WT)) and age (4 and 12 months). Uptake of ^{99m}Tc-HMPAO was normalized to mean brain uptake (n=4).

Figure 2: Elderly SCL5A8-deficient mice (KO) present diffuse leucoencephalopathy characterized by intramyelinic oedema without myelin loss but associated with microglial activation. Hematoxylin, Eosin and Safran (H&E) and (LBF) coloration of paraffin-embedded sections of cerebellum from control and SLC5A8-deficient mice (KO) (optical microscopy ×10) **(A)**. LBF coloration of white matter tract fibers in the brainstem of SLC5A8-deficient mice (KO) (×40) **(B)**. NeuN and Olig2 immunohistochemcal staining in elderly control (WT) and SLC5A8-deficient mice (KO) cerebellum and brain cortex (×10) **(C)**. Iba1-specific immunostaining in control and slc5a8-deficient mice corpus callosum and cerebellum (×40; ×10) **(D); n= 6**. Scale bar 100 μm.

Figure 3: SLC5A8 expression is not detected in the mouse brain but is detected in renal proximal tubules. Immunohistochemistry with an anti SLC5A8-specific antibody in control and in SLC5A8-deficient mice cerebellum **(A)** and kidney **(B)** ; Renal glomeruli **(g), n=6**. Scale bar 100 μM.

Figure 4: SLC5A8-deficient mice present β-hydroxybutyrate deficiency due to a renal reabsorption defect in proximal tubular tubule. Level of hydroxybutyrate [M-H] m/z: 103.0387 (see **Extended data Figure 4-2**) **(A)** and its acyl carnitine [M+H] m/z: 248.1492 (see

Extended data Figure 4-3) **(B)** in 24-hour urine of wild-type and SLC5A8-deficient mice assessed by LC-MS (n=4).

Figure 5: Depletion of β-hydroxybutyrate ([M-H] m/z: 103.0387) levels in brain tissue of SLC5A8-deficient mice assessed by LCMS. Measurements were performed on crushed fresh brain tissue of older mice (24 months) (n=5) **(A)** and from rostral-mesencephalon frozen sections of young mice (3 months) (n=4) **(B).** Frozen sections were analyzed whole and after micro-dissection of the neocortex (grey matter) and the mesencephalon (white matter) as specified on the cutting plane below.

Figure 6: Elderly SLC5A8-deficient mice present insulin-resistance. Glucose Tolerance Test (GTT) with 3-month-old and 18-month-old, control and SLC5A8-deficient mice (n=5) **(A)**. Insulin Tolerance Test (ITT) with 18-mont-old SLC5A8-deficient mice (n=6) **(B)**.

Figure 1

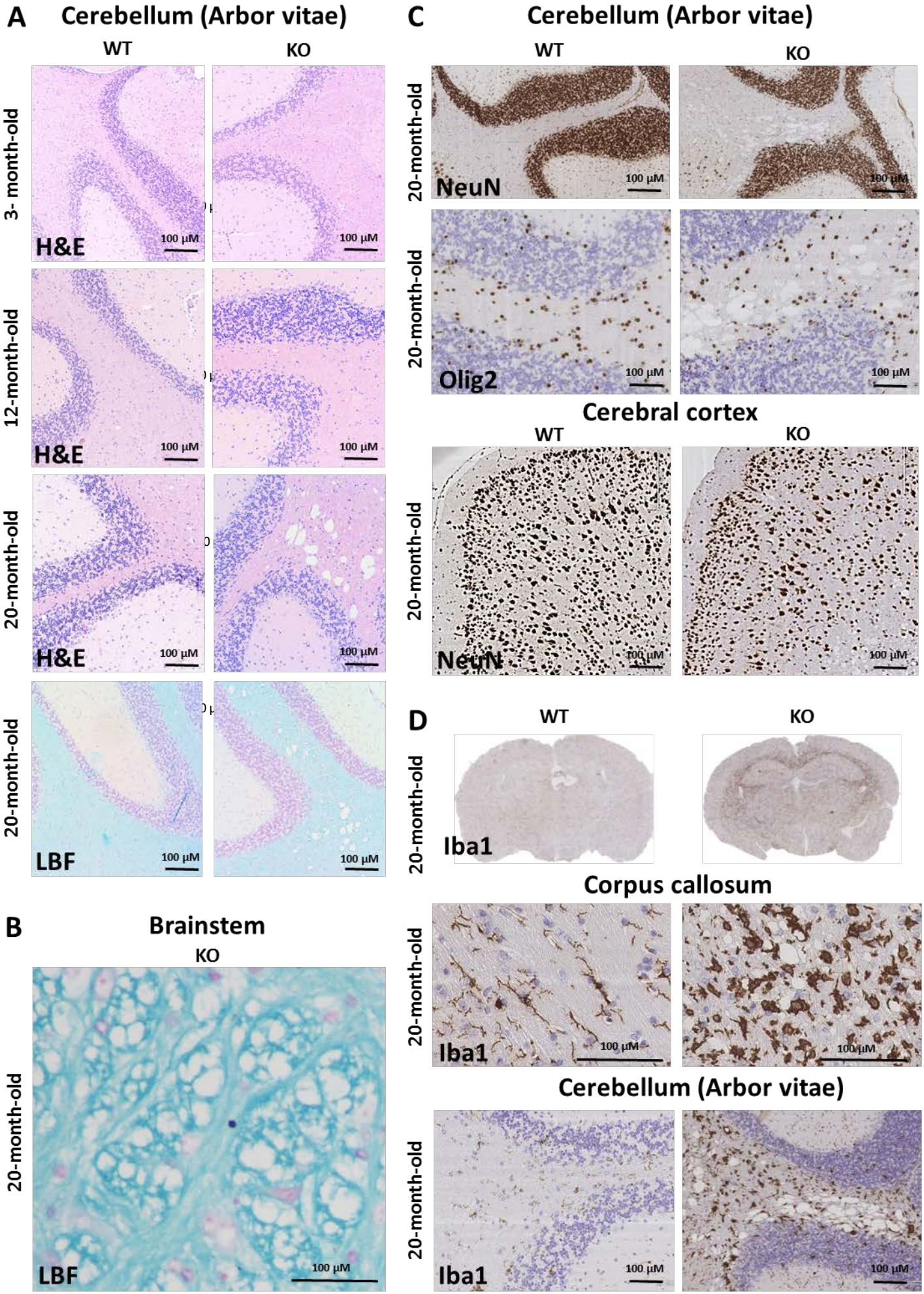
A
Cerebellum (Arbor vitae)
WT
KO
3- month-old
12-month-old
20-month-old
20-month-old
H&E
H&E
H&E
LBF
100 µM
B
Brainstem
KO
20-month-old
LBF
100 µM
C
Cerebellum (Arbor vitae)
WT
KO
20-month-old
NeuN
Olig2
Cerebral cortex
NeuN
D
WT
KO
20-month-old
Iba1
Corpus callosum
Iba1
Cerebellum (Arbor vitae)
Iba1

Figure 2

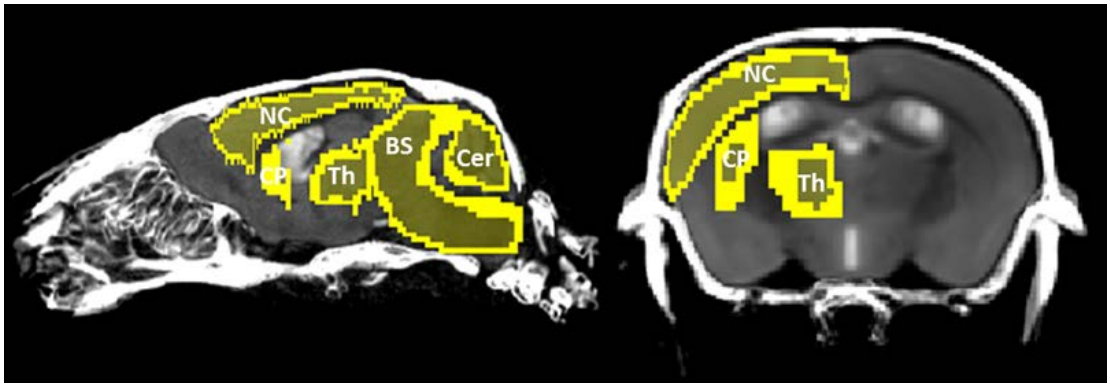
NC
CP
Th
BS
Cer
NC
CP
Th

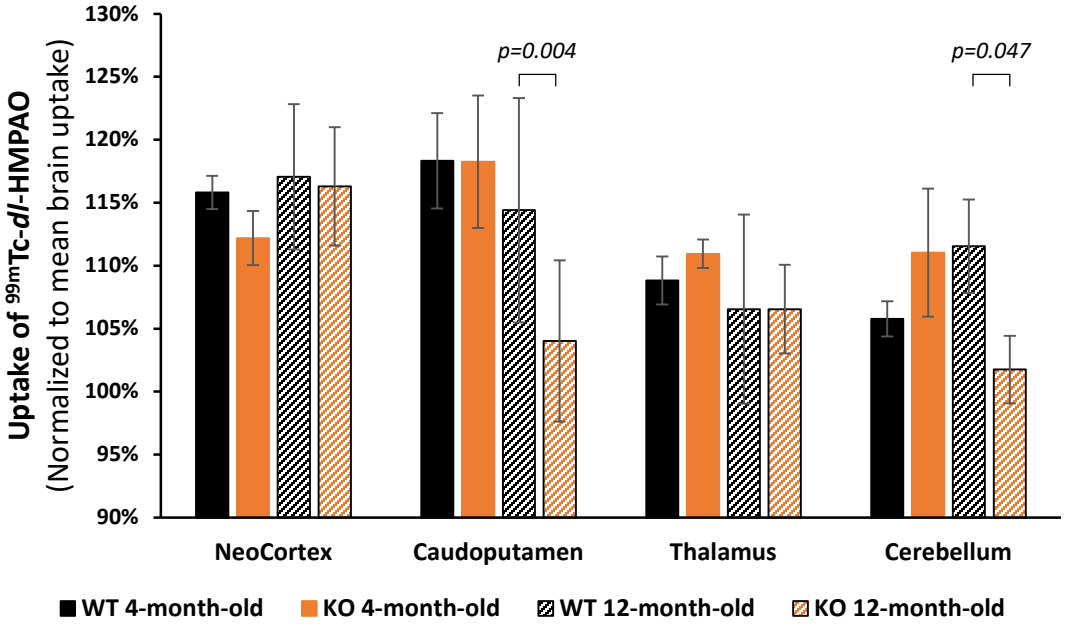
Uptake of 99mTc-dl-HMPAO
(Normalized to mean brain uptake)
130%
125%
120%
115%
110%
105%
100%
95%
90%
p=0.004
p=0.047
NeoCortex
Caudoputamen
Thalamus
Cerebellum
WT 4-month-old
KO 4-month-old
WT 12-month-old
KO 12-month-old

Figure 3

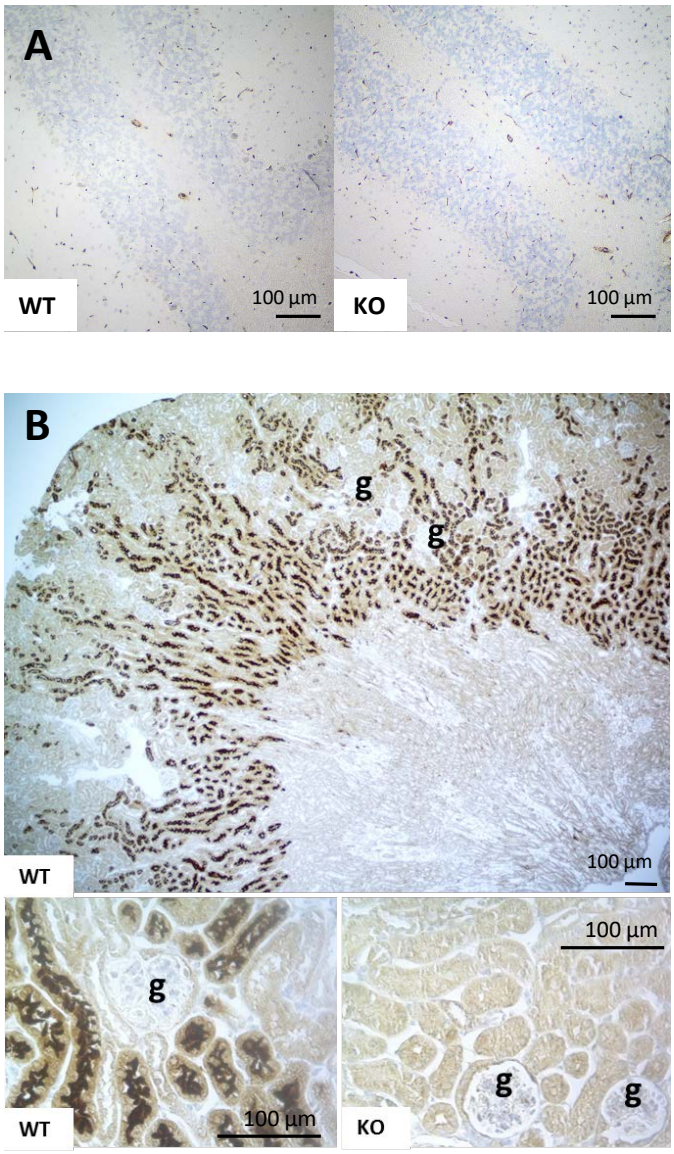

Figure 4

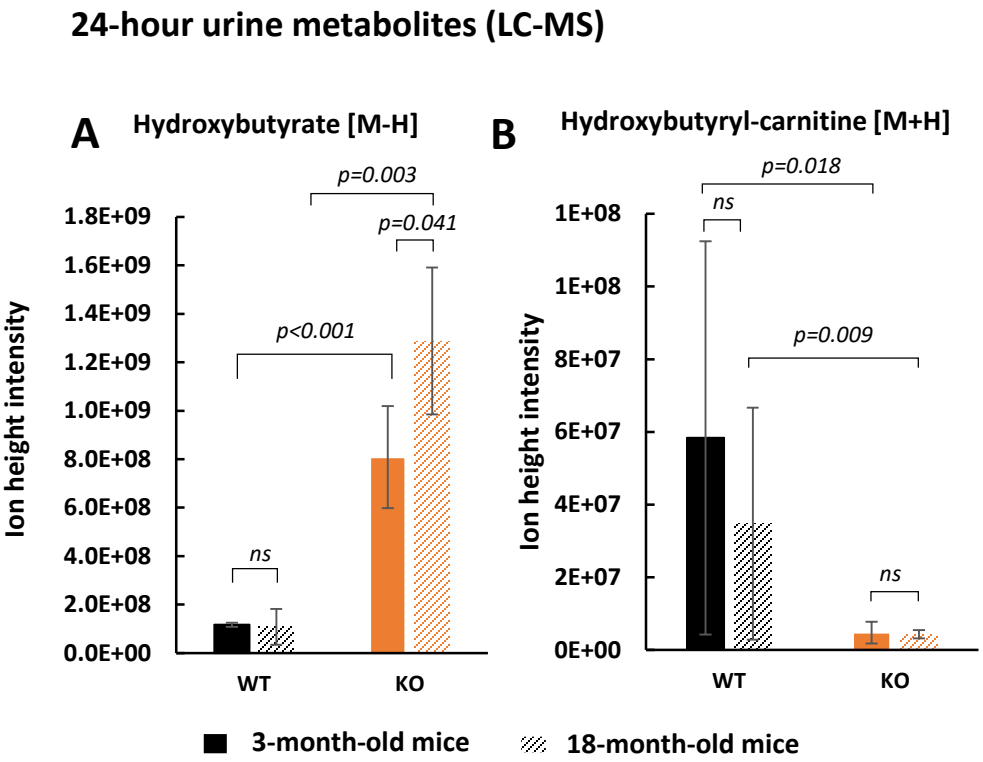
24-hour urine metabolites (LC-MS)
A
Hydroxybutyrate [M-H]
Ion height intensity
1.8E+09
1.6E+09
1.4E+09
1.2E+09
1.0E+09
8.0E+08
6.0E+08
4.0E+08
2.0E+08
0.0E+00
p=0.003
p=0.041
p<0.001
ns
WT
KO
B
Hydroxybutyryl-carnitine [M+H]
Ion height intensity
1E+08
1E+08
8E+07
6E+07
4E+07
2E+07
0E+00
p=0.018
ns
p=0.009
ns
WT
KO
3-month-old mice
18-month-old mice

Figure 5

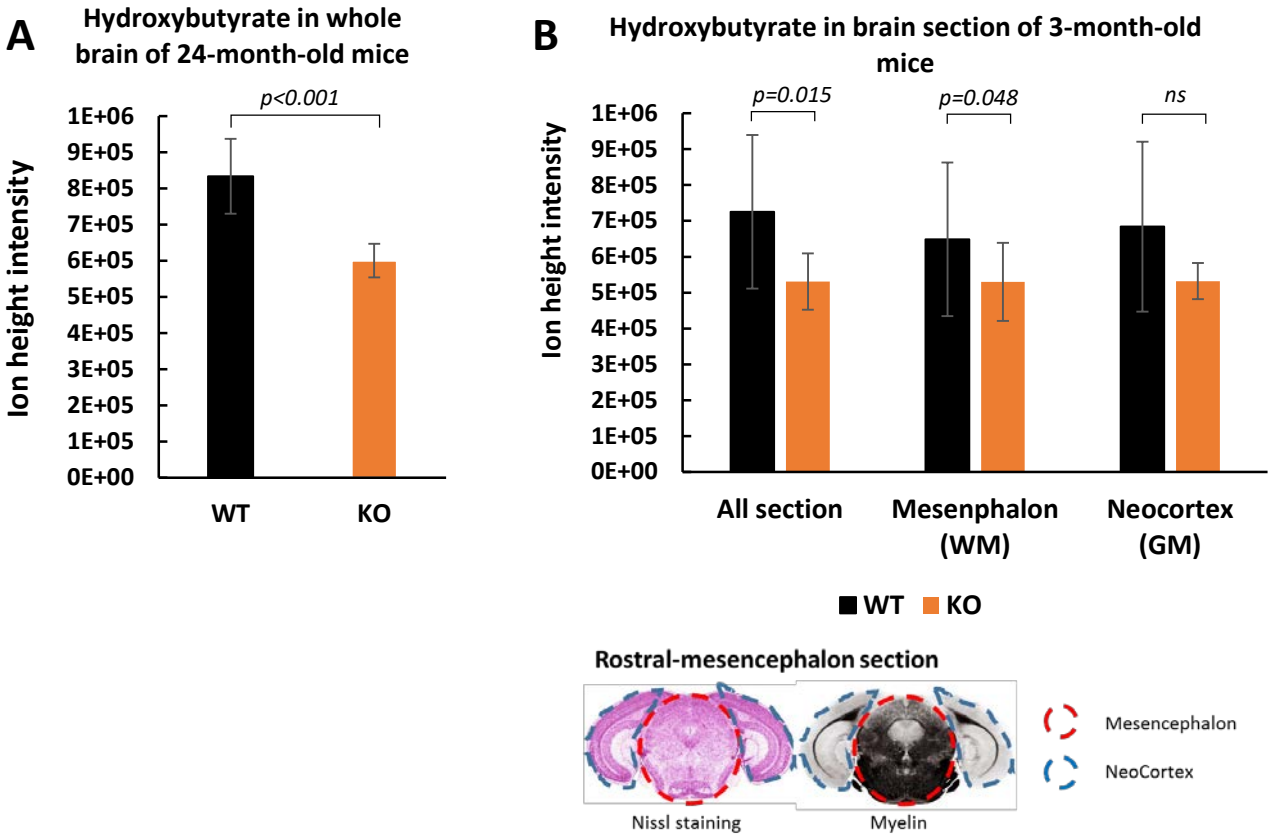
A
Hydroxybutyrate in whole brain of 24-month-old mice
p<0.001
Ion height intensity
1E+06
9E+05
8E+05
7E+05
6E+05
5E+05
4E+05
3E+05
2E+05
1E+05
0E+00
WT
KO
B
Hydroxybutyrate in brain section of 3-month-old mice
p=0.015
p=0.048
ns
Ion height intensity
All section
Mesenphalon (WM)
Neocortex (GM)
WT
KO
Rostral-mesencephalon section
Mesencephalon
NeoCortex
Nissl staining
Myelin

Figure 6

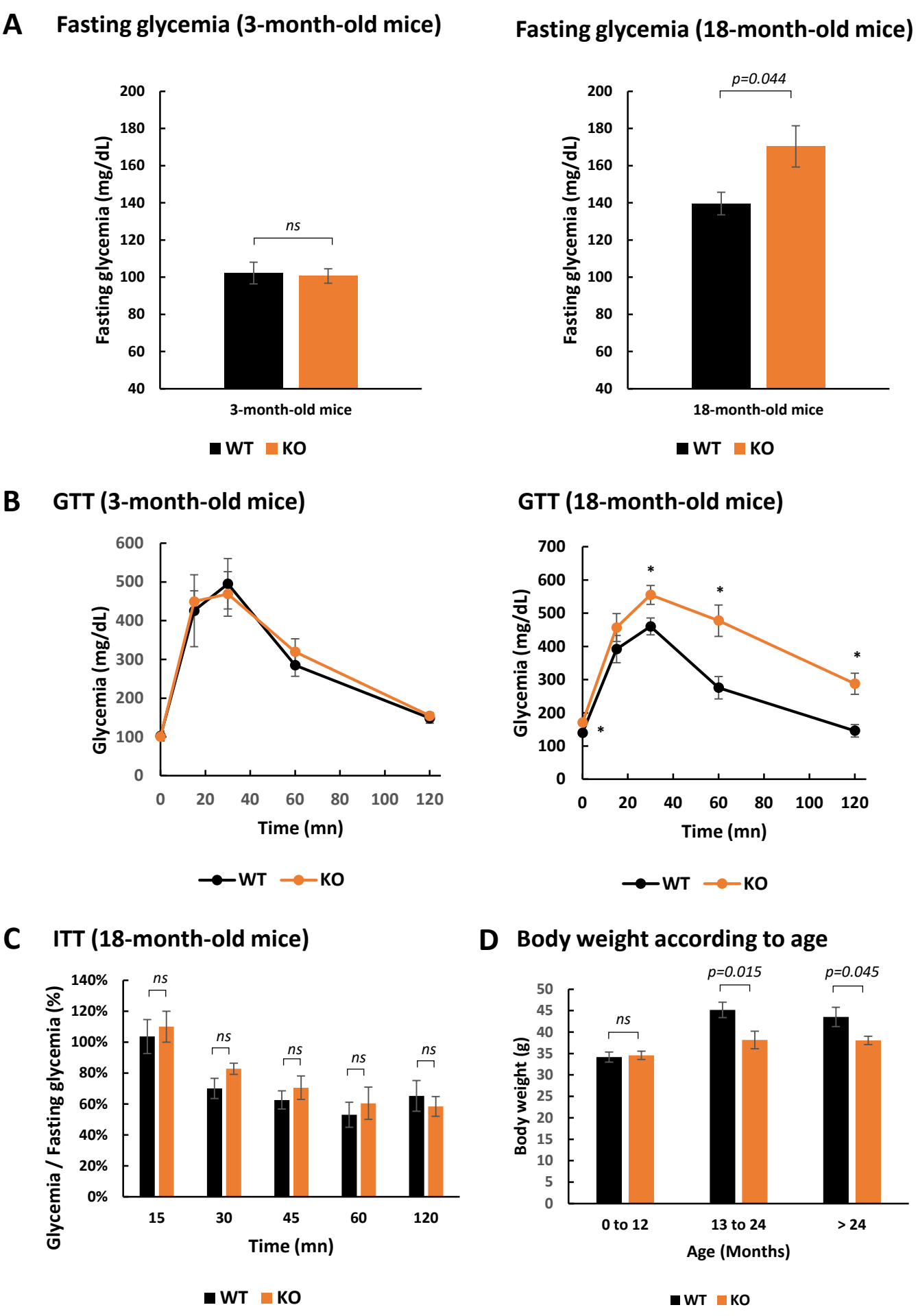
A
Fasting glycemia (3-month-old mice)
Fasting glycemia (mg/dL)
200
180
160
140
120
100
80
60
40
ns
3-month-old mice
WT KO
Fasting glycemia (18-month-old mice)
p=0.044
18-month-old mice
WT KO
B
GTT (3-month-old mice)
Glycemia (mg/dL)
600
500
400
300
200
100
0
0 20 40 60 80 100 120
Time (mn)
WT KO
GTT (18-month-old mice)
700
600
500
400
300
200
100
0
*
0 20 40 60 80 100 120
Time (mn)
WT KO
C
ITT (18-month-old mice)
Glycemia / Fasting glycemia (%)
140%
120%
100%
80%
60%
40%
20%
0%
ns
15 30 45 60 120
Time (mn)
WT KO
D
Body weight according to age
Body weight (g)
50
45
40
35
30
25
20
15
10
5
0
ns
p=0.015
p=0.045
0 to 12
13 to 24
> 24
Age (Months)
WT KO

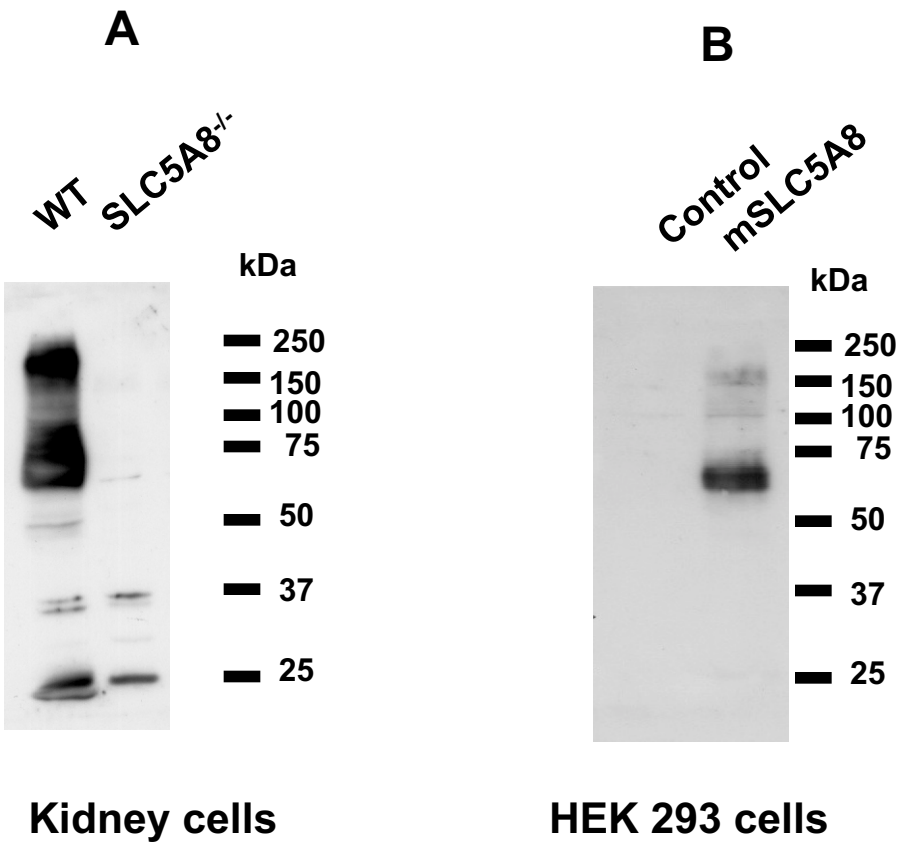

Supplementary figure 1. Western blot analysis of SLC5A8 expression. These membranes were probed with 4R (2.32 mg/L) for mSLC5A8. 4R is an in house rat monoclonal antibody, raised against mouse SLC5A8 544-610 peptide. (**A**) Western blot analyses were performed on membrane vesicles from kidney cells of control mice (Lane WT) or SLC5A8-deficient mice (Lane SLC5A8$^{-/-}$). Membrane vesicles were prepared, proteins (25 µg) were separated on SDS gels and transferred onto PVDF membranes as previously described (Huc-Brandt et al, 2011, Biochim Biophys Acta.;1808:65-77). (**B**) Western blot analyses were conducted on non-transfected HEK 293 cells (Lane Control) or transfected HEK 293 cells with the mouse SLC5A8 encoding plasmid (Lane mSLC5A8). Proteins (30 µg) were separated on SDS gels and transferred onto PVDF membranes.

Urine analysis

m/z	Retention time	HMDB ID	Name	Monoisotopic mass	Adduct	Adduct m/z	Delta (ppm)	MS2 Validation
103.0387	1.12	HMDB0000011	**Hydroxybutyric acid**	104.0473	[M-H]	103.0401	13	Yes

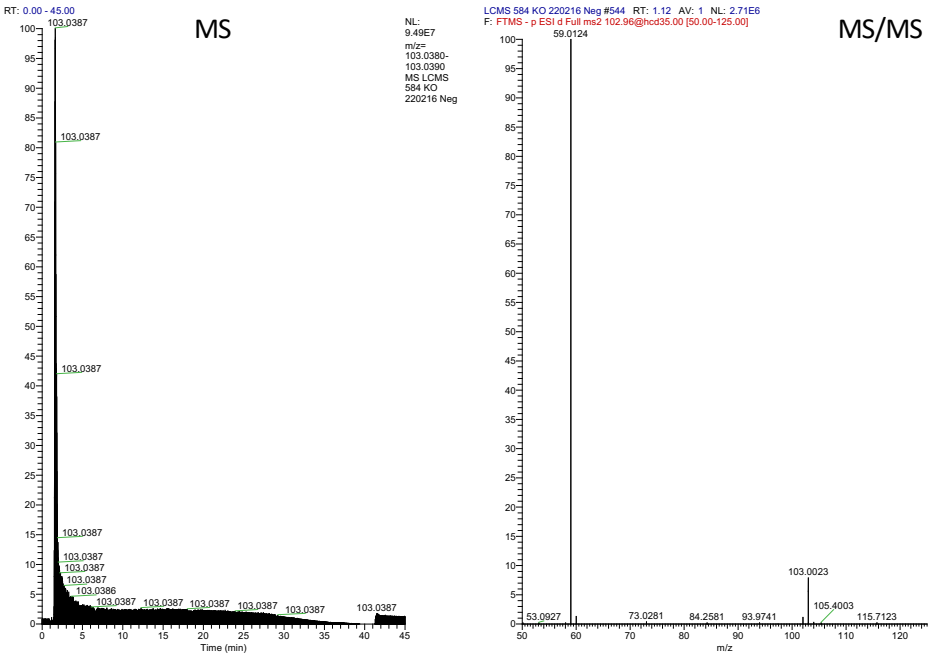

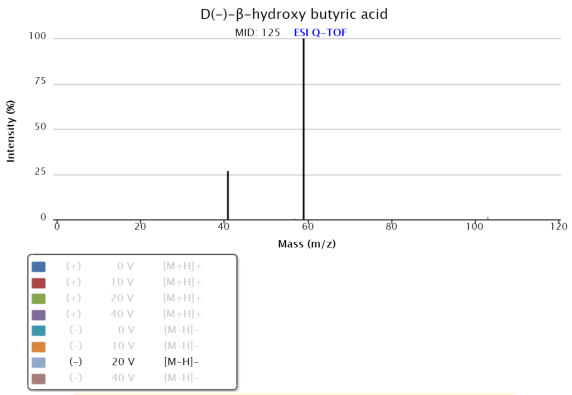

METLIN metabolomics database source

Supplementary figure 2. Mass spectrometry identification of β-hydroxybutyrate.

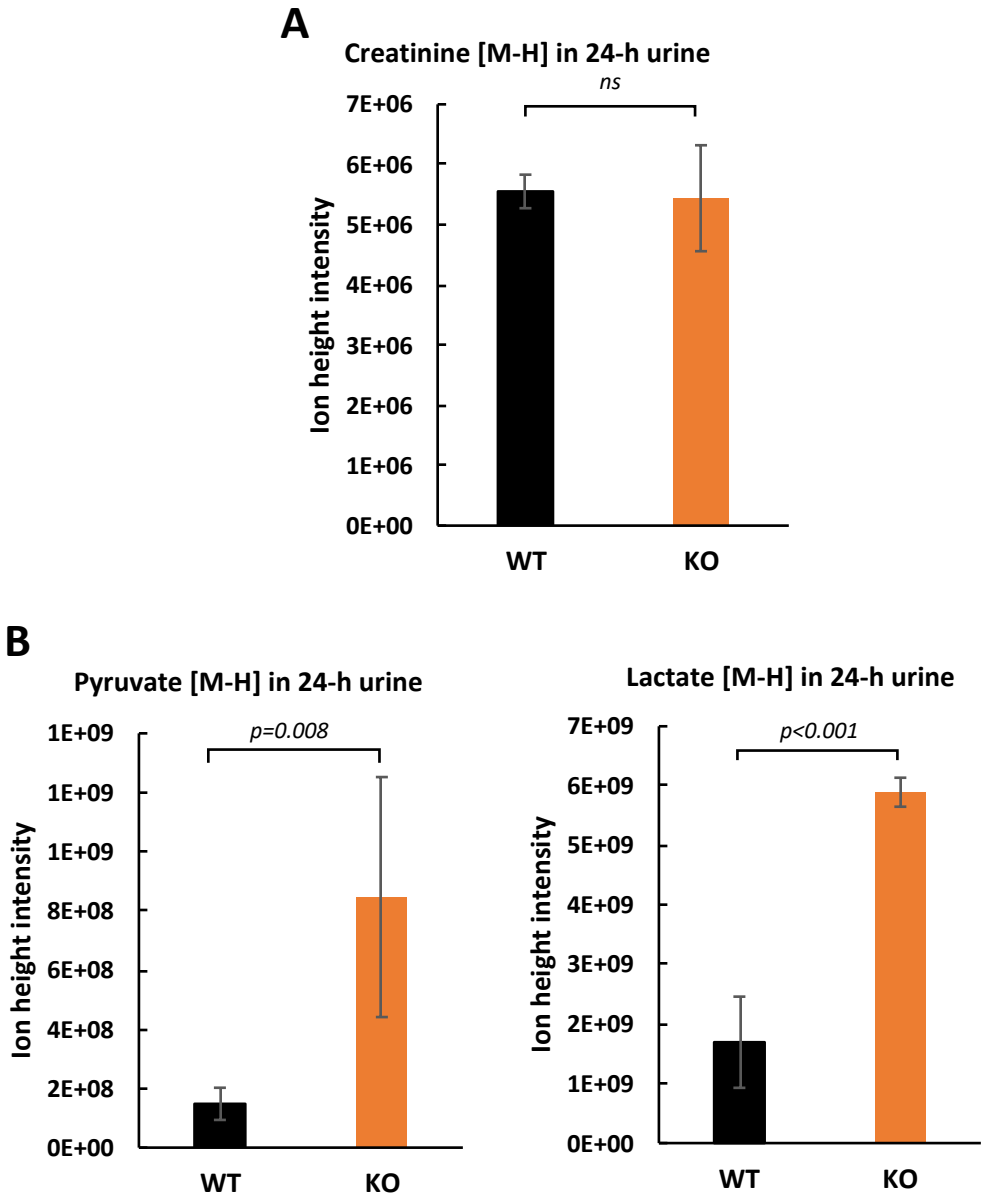

Supplementary figure 3. Level of creatinine [M-H] m/z: 112.0503 (A), pyruvate [M-H] m/z: 87.0073 and lactate [M-H] m/z: 88.0230 (B) in 24-hour urine of 3-month-old wild-type (WT) and 3-month-old SLC5A8-deficient (KO) mice assessed by LC-MS (n=4).

Urine analysis

m/z	Retention time	HMDB ID	Name	Monoisotopic mass	Adduct	Adduct m/z	Delta (ppm)	MS2 Validation
248.1492	2.01	HMDB0013127	**Hydroxybutyrylcarnitine**	247.1420	[M+H]	248.1492	0	Yes

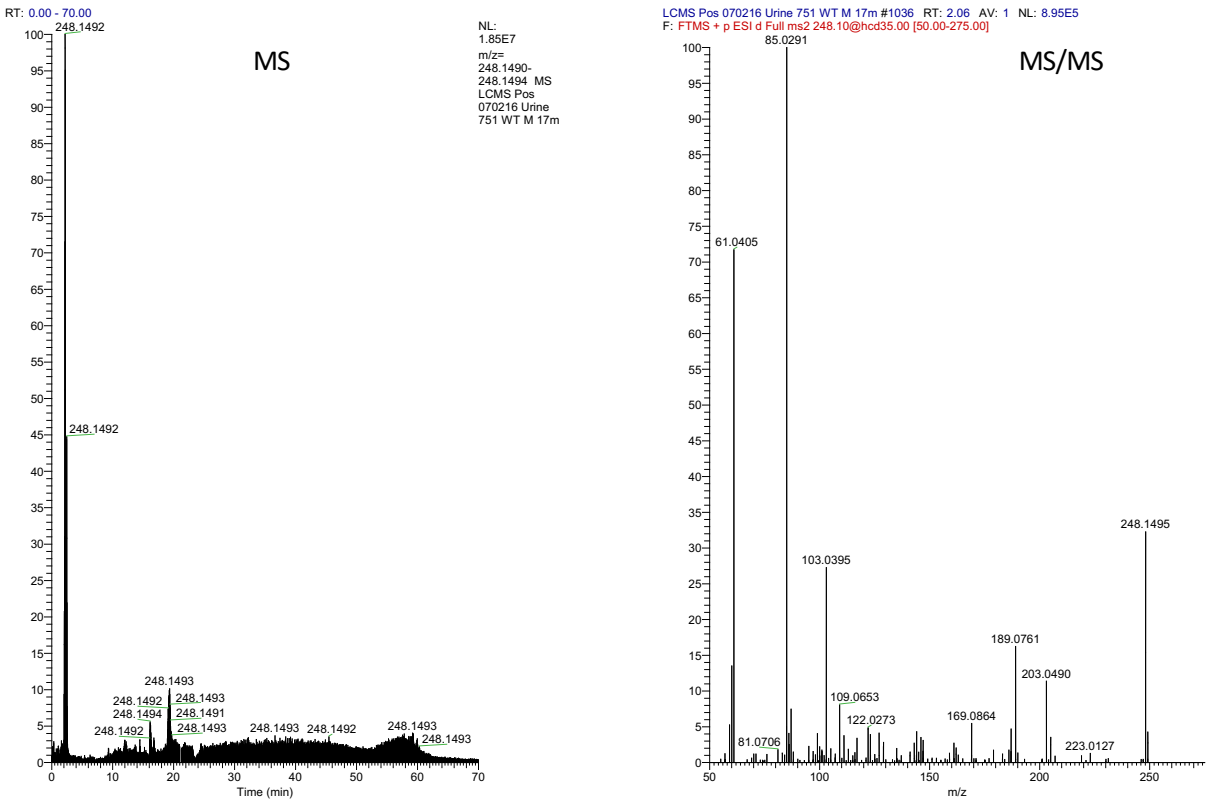

Supplementary figure 4. Mass spectrometry identification of acyl carnitine.